Articles

Influence of the Support in the Selectivity of Ni/Clay Catalysts for Vegetable Oil Hydrogenation

J. A. Anderson,* M. T. Rodrigo, L. Daza, and S. Mendioroz

Instituto de Catálisis y Petroleoquimica, CSIC, Campus UAM, Cantoblanco, 28049 Madrid, Spain

Received August 14, 1992. In Final Form: January 19, 1993®

Two naturally occurring clays of Spanish origin, bentonite and palygorskite, have been used as support material for nickel hydrogenation catalysts in which the active phase has been deposited by means of the precipitation method. The structural and textural characteristics of the supports have been studied by XRD, N_2 adsorption/desorption, and mercury porosimetry and the acid sites determined by thermogravimetry and infrared studies of adsorbed pyridine. The Ni phases present were characterized by XRD, TEM, XPS, FTIR of adsorbed CO, and the degree of reduction determined thermogravimetrically. XRD and TEM indicate Ni particle size to be equivalent for both supports although the detection by FTIR of a high proportion of bridging CO for the bentonite support suggests the presence of addition small particles for this support which may be located between lamellae. These smaller particles are consistent with the more difficult reduction of Ni in this support. Although activity for the hydrogenation of sunflower oil was similar for both catalysts, significant differences regarding the selectivity have been observed which may be attributed to the differences in morphology of the support materials. Mass transport limitations resulting from reaction of linoleic acid at Ni sites between lamellae of bentonite, leads to consecutive hydrogenation through to stearic acid, whereas the palygorskite supported catalyst remained highly selective to oleic acid even at high conversion levels.

Introduction

The hydrogenation of vegetable oils is of special interest in the processes of modification of edible fats and oils. The aim of the process being to increase the stability of polyunsaturated fats by the partial or total saturation of the double bonds. This process results in important chemical and nutritional modifications in addition to an improvement in the preservation to the hydrogenated product.

The catalyst currently used for the industrial hydrogenation process is supported nickel. Normally, the supports used are silica[1] and carbon,[2] although recently natural silicates such as sepiolite[3] and diatomite[4] have been studied for this process. Additionally, aluminosilicates and in particular montmorillonite and its pillared derivatives have been used.[5] With this type of catalyst, studies of the influence of reduced nickel content, metal dispersion and particle size on catalytic activity have been conducted.[6] The influence of pore size on selectivity has also received attention.[6,7] However the influence of the support morphology on the reaction is not known. The objective of the current article is to complete studies regarding the influence of the support in the reaction of the hydrogenation of vegetable oils taking into account the morphology of the support and the active centers of the catalyst. For this purpose, two naturally abundant silicates of different morphologies, bentonite and palygorskite, have been selected. Bentonite is a clay material consisting essentially of smectites and in particular montmorillonite. It is a laminar silicate of the type 2:1, that is consisting of a sheet of octahedral alumina between two sheets of tetrahedral silica around 10 Å thick. Montmorillonite is susceptible to isomorphous substitution of cations in both tetrahedral and octahedral environments. The most common are substitution of Si^{4+} by Al^{3+} in tetrahedral positions and Al^{3+} by Mg^{2+} in octahedral positions resulting in negative charges in the silicate laminas. This excess charge is compensated by the presence of hydrated cations which are situated between the laminas and which may be readily substituted. The general formula of montmorillonite,[8] considering half of the unit cell and without substitutions is

$$(Si_4)_T(Al_{2-\gamma}Mg_\gamma)_O O_{10}(OH)_2(M^+_{\gamma}\cdot nH_2O)_{cc}$$

The palygorskite structure was first determined by Bradley[9] and consists of fibers which contain two rows of silica tetrahedrons between a central magnesium with octahedral coordination. Due to the position of the unshared vertices of the tetrahedral between the rows, capillary channels of dimensions 9 × 5.3 Å exist, orientated in the longitudinal direction of the fibers, and which may be penetrated by water and other fluids. In accordance with this structure, the formula of palygorskite is $Si_8Mg_5O_{20}(OH)_2(H_2O)_4\cdot 4H_2O$, in which the silicon and magnesium tetrahedral and octahedral vacancies, respectively, can be filled by other elements. These isomorphous substitutions result in the laminar charges present in the

® Abstract published in *Advance ACS Abstracts,* August 15, 1993.

(1) Gut, G.; Kosinka, J.; Prabucki, A.; Schuerch, A. *Chem. Eng. Sci.* **1979**, *34*, 1051.
(2) Chung, Ch.; Winterbottom, J. M. *J. Chem. Technol. Biotechnol.* **1987**, *38*, 15.
(3) Corma, A.; Mifsud, A.; Pérez Pariente, J. *Ind. Eng. Chem. Res.* **1988**, *27*, 2044.
(4) Muñoz, V.; Mendioroz, S. *Appl. Catal.* **1990**, *66*, 73.
(5) Occelli, M. L. *Ind. Eng. Chem. Process Res. Dev.* **1983**, *22*, 553.
(6) Coenen, J. W. E. *Ind. Eng. Chem. Fundam.* **1986**, *25*, 43.
(7) Colen, G. C. M; van Duijn, G.; van Oosten, H. J. *Appl. Catal.* **1988**, *43*, 339.
(8) Martin Vivaldi, J. L. *Clays Clay Miner.* **1963**, *11*, 327.
(9) Bradley, W. F. *Am. Miner.* **1940**, *25*, 405.

0743-7463/93/2409-2485$04.00/0

silicate.[10] The substitution of Si^{4+} in the tetrahedral position is almost exclusively restricted to Al^{3+}, while the octahedral may have a more heterogeneous composition, Al^{3+} being the most common substituted ion. Fundamentally, the material may be treated as a magnesia-alumino silicate.[11]

Experimental Section

Raw Materials. Bentonite (BT) from Almeria (Spain) and palygorskite (PS) from Cáceres (Spain) were used throughout this study. Nickel nitrate from Prolabo (97%) and urea from Panreac (99%) were used in the catalyst preparations.

Catalyst Preparation. Nickel was deposited by means of the precipitation method as described by van Dillen et al.[12] To a 0.13 M solution of nickel nitrate, 10 g of support was added and the pH adjusted to 3.5 by the addition of nitric acid. This was then heated to 363 K before addition of 0.4 M urea which led to a controlled preciptation of hydroxide over the support. After 6 h, the suspension was filtered, washed with distilled water, and then dried at 383 K for 16 h prior to reduction. The precursors were reduced in two stages: an initial treatment at 573 K for 2 h in a H_2 flow of 100 cm^3 min^{-1}, and secondly at 773 K for 2 h in a H_2 flow at 100 cm^3 min^{-1}. The degree of reduction of nickel (α) was determined thermogravimetrically by firstly heating the sample in a H_2 flow (80 cm^3 min^{-1}) to 773 K at 10 K min^{-1} followed by oxidation in air under the same conditions.

Characterization Techniques. Textural analyses were performed by nitrogen adsorption/desorption isotherms at 77 K and by mercury intrusion porosimetry using a Micromeritics Digisorb 2600 and Pore-Sizer 9310, respectively. BET surface areas were calculated at relative pressures p/p_0 below 0.3 and taking 0.162 nm^2 as the cross-sectional area of the nitrogen molecule.

The nickel content of the catalysts was determined using a Perkin-Elmer 3030 atomic absorption spectrophotometer, following acid digestion of the samples in a PTFR autoclave following the method of Langmhyr and Paus.[13] X-ray diffraction (XRD) measurements were conducted using powdered samples with a Rigaku generator and rotating anode, coupled to a Rigaku diffractometer. Cu Kα radiation was used and a scan speed of 2 deg min^{-1}. Thermal analysis (TG), temperature programmed reduction (TPR), and pyridine adsorption–desorption experiments were carried out using a Perkin-Elmer TGS II thermobalance coupled to a system 7/4 thermal controller and 3600 data station. For the analysis of the quantity of surface acid centers as determined by TG, the following sequence of treatments were conducted: (i) the sample was initially outgassed at temperatures up to 773 K and then cooled and subsequently exposed to a flow of N_2 saturated with pyridine vapor for 3 h at 298 K, during which the adsorption of pyridine was registered by the increase in weight; (ii) at the same temperature, N_2 was passed over the sample for 3 h to eliminate physically adsorbed pyridine; (iii) the sample was then heated in N_2 at a rate of 10 K min^{-1} to 773 K to eliminate the pyridine chemisorbed at the acidic centers of the catalyst surface and losses in weight registered as a function of temperature to calculate the number of micromoles of pyridine adsorbed per gram of catalyst and to gain information regarding the relative strengths of adsorbed pyridine.

Infrared experiments were conducted using a portable glass infrared cell fitted with KBr windows and using an external furnace for heat treatments. Catalyst samples were presented in the form of self-supporting wafers (10 and 20 mg cm^{-2} for PSP and BTP, respectively) and evacuated at ambient temperature for 16 h. The prereduced samples were further reduced in situ in a flow of hydrogen (60 cm^3 min^{-1}) by firstly ramping the temperature to 573 K and then maintaining this temperature for 1 h. The temperature was then increased to 673 K and held at this temperature for 2 h. Samples were degassed at this temperature for 15 min in dynamic vacuum, cooled to ambient temperature, and then exposed to the adsorbate gas or vapor after recording a spectrum of the background prior to adsorption. Apart from spectra shown of the OH region, 3800–3400 cm^{-1}, all spectra shown here were obtained by subtraction of the background spectra. Spectra were recorded using a Nicolet 5ZDX spectrometer at a resolution of 4 cm^{-1} and were averaged over 100 scans.

The metal particle size was determined by transmission electron microscopy (TEM) using a Phillips 300 apparatus, and from line broadening in XRD diffractograms using the (111) line of Ni at 22.3°. The metal surface area was calculated from the average metal particle size[14] using the expression $S_{Ni} = 5/\rho\, d_{Ni}$, where ρ is the density of the metal (8.9 g cm^{-3}) and taking into account the degree of reduction (α) in the samples.

Catalyst Testing. Catalytic studies were conducted in a discontinuous spherical glass reactor of total volume 500 cm^{-3}. A thermal blanket and thermocouple maintained the reactor temperature within ±2 K at 453 K. Other reaction conditions were: total pressure 101.325 kN m^2, H_2 flow 200 cm^{-3} min^{-1}, stirring rate 1400 rpm, particle size 0.3 mm and 0.05% (w/w) Ni with respect to the amount of oil (100 g per experiment). Before these conditions were selected, various tests were carried out to ensure the absence of control by internal or external diffusion. Internal intraparticular diffusion was detected only for particle sizes above 0.8 mm. By use of stirring speeds between 600 and 1800 rpm, a difference of less than 3% in reaction rate was found for speeds above 1200 rpm. In the range of catalyst weight, 0.05–0.2 g, a plot of the inverse of reaction rate against the inverse of catalyst mass gave a straight line. Additionally, in the range 453–473 K, the activation energy for the reaction was calculated as 44.4 kJ mol^{-1}, indicating chemical control of the reaction. The order of reaction was found to be zero, and plots of lioleic acid concentration versus time were linear up to approximately 75% conversion. Catalytic activities were calculated from the gradients of the linear portions of the lines in these plots. Refined commercial sunflower seed oil (acidity 0.2°) with a composition in acids of palmitic 7%, stearic 5%, oleic 29%, and linoleic 59%, was used throughout. Oil samples were analyzed by GLC using a packed column of 20% DGES over Chromosorb B and heated isothermally to 343 K. Prior to analysis, the triglycerides were converted into methylesters,[15] using tetramethylammonium hydroxide (TMAH), as a catalyst.

Table I. Chemical Composition of Bentonite and Palygorskite

	% weight	
constituent	bentonite	palygorskite
SiO_2	56.58	53.41
Al_2O_3	14.42	10.94
MgO	3.50	7.42
Na_2O	0.16	0.82
CaO	0.84	0.12
K_2O	0.13	0.92
Fe_2O_3	2.40	3.92
$CO_2 + H_2O$	21.97	21.95

Results and Discussion

Characterization of Supports. The chemical composition of the two support materials, as determined by atomic absorption is shown in Table I. The content of silica in both samples is of the same order. The mineralogical composition of the samples was determined by the presence and relative intensities of various peaks in the XRD diffractograms (Figure 1). In the case of the bentonite sample, characteristic peaks[16] of montmorillonite were observed at 15.50, 4.50, 3.75, 2.55, 2.25, and 1.69

(10) Tarasevish, V. I.; Kats, B. M.; Malinovskic, E. C. *Colloid J. USSR* **1984**, *46*, 140.
(11) González, F.; Pesquera, C.; Benito, I.; Mendioroz, S.; Pajares, J. A. *Bol. Geol. Min.* **1989**, *100*, 86.
(12) van Dillen, J. A.; Geus, J. W.; Hermans, L. A. M.; van der Meijden, J. *Proc. Int. Cong. Catal. 6th* **1976**, 677.
(13) Langmyhr, F. J.; Paus, P. E. *Anal. Chim. Acta* **1968**, *43*, 397.
(14) Anderson, J. R. *Structure of metallic catalysts*; Academic Press: London, 1975; p 469.
(15) Metcalfe, L. D.; Wang, C. N. *J. Chromatogr. Sci.* **1981**, *19*, 530.
(16) Brown, G. *The X-Ray identification and crystal structure of clays minerals*; Mineralogical Society: London, 1961; p 544.

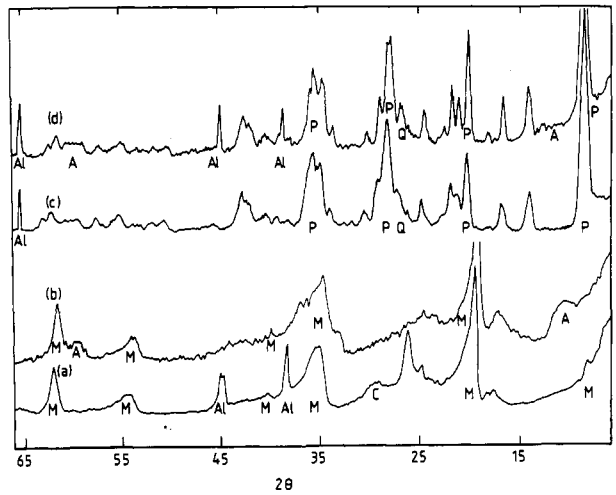

Figure 1. XRD pattern for Bentonite (a) before and (b) after incorporation of nickel and for palygorskite (c) before and (d) after incorporation of nickel: A, antigorite; Al, aluminum (base plate used); C, calcite; M, montmorillonite; P, palygorskite; Q, quartz.

Table II. Textural Characteristics of Supports and Catalysts

	bentonite	palygorskite	BTP	PSP
S_{BET} (m^2/g)	75	71	83	77
V_p[a] (cm^3/g)	0.10	0.14	0.14	0.25
r_p[b] (Å)	27	39	35	65
V_M[c] (cm^3/g)	0.38	1.41		
R_M[d] (Å)	101	397		

[a] Pore volume from N_2 uptake at $p/p_0 = 0.98$. [b] Average mesopore radius. [c] Macropore volume from mercury intrusion. [d] Average pore radius from mercury intrusion.

Å (Figure 1a). A peak appearing at 3.02 Å indicates traces of calcite, and the sharp peak at 1.50 Å is indicative of the mineral in the dioctahedral form. For palygorskite,[17] the most intense peaks were at 10.32, 4.46, 3.21, and 2.56 Å (Figure 1c). The small peak at 3.33 Å is due to the presence of quartz. The mineral was therefore of a high purity with a composition of 95% palygorskite, 5% mica, and traces of quartz.

Experiments were conducted by degassing the samples at temperatures in the range 298–773 K for 16 h until obtaining a final vacuum of 10^{-6} Torr and then measuring the BET surface area. For bentonite, no influence of thermal pretreatment occurs, with a surface area of approximately 75 $m^2\ g^{-1}$ being measured throughout the temperature range. In the case of palygorskite, values of 153 (298 K), 115 (373 K), and 71 $m^2\ g^{-1}$ (423 K) were obtained and due to the "folding" of fibers which occurs below 423 K, a stable surface area of 71 $m^2 g^{-1}$ was measured for degassing temperatures up to 773 K. The textural characteristics of both support materials are summarized in Table II. These data are for samples following evacuation at 423 K, this being above the temperature in which folding of the fibers in palygorskite takes place and above which no further loss in surface area occurs up to 773 K. Bentonite presents an adsorption–desorption N_2 isotherm of type IV of the classification BDDT, typical of mesoporous materials with a hysteresis loop type H3 due to nonrigid slit-shaped pores among lamellae.[18] The isotherm for palygorskite shows a hysteresis loop not well defined, due to a mixture of types H1 and H3 corresponding to interparticulate porosity, mainly cylindrical in shape, which is produced by a clustering of the individual fibers of the palygorskite, leaving capillary spaces between them.

Table III. Characteristics of Ni/Clay Catalysts

catalyst	Ni (wt %)	α[a] (%)	d_{TEM}[b] (Å)	d_{XRD}[c] (Å)	S_M[d] (m^2/g)	acidity (μmol/g)
BTP	9.4	87	110	112	44	420
PSP	8.5	98	102	105	54	360

[a] Degree of metal reduction. [b] Average particle diameter from TEM. [c] Particle diameter from XRD line broadening. [d] Metal surface area calculated from average particle diameter and degree of reduction.

Characterization of Catalysts. The textural characteristics of the supported Ni catalysts following reduction at 773 K are summarized in Table II and the modifications resulting from the metal incorporation obtained by comparing the data with those for the Ni-free supports. The specific BET area was increased by 10.6% in the case of the bentonite and 8.5% for the palygorskite, as a result of incorporation of the active phase. The average pore radius and pore volume were increased for both materials, although particularly in the case of palygorskite, following Ni incorporation.

Nickel contents as determined by atomic absorption were 9.4 and 8.5% for the catalysts supported by bentonite (BTP) and palygorskite (PSP), respectively (Table III). These nickel contents are approximately proportional to the silica content in supports, with molar ratios of 0.17 for BTP and 0.16 for PSP suggesting the formation of a common precursor in both samples. The XPS atomic ratio of Ni/Si for BTP was also 0.17, indicating the nickel precursor to be evenly distributed throughout the support surface, i.e. Ni between the layers. In the case of PSP, the Ni/Si ratio determined by XPS was 0.25, indicating a higher concentration of Ni deposited on the external layer within the escape depth of the photoelectron. It is known that the precipitation of nickel over silica, using urea, leads to the formation of nickel hydrosilicate.[12,19,20] Such a hydrosilicate is characterized by its layered structure, which when formed in an appreciable quantity leads to considerable textural changes in the support.[12,20] These textural changes are entirely consistent with the data contained in Table II, with the increases in BET surface area of the same order as those previously reported for Ni/SiO_2 catalysts.[20] XRD patterns of the supported catalysts prior to reduction (Figure 1 b,d) show peaks at 7.43 and 1.54 Å characteristic of the antigorite structure, $Ni_3(OH)_4Si_2O_5$.[21] In agreement with previous reports[12,20] the XRD pattern of this phase is not clearly defined due to its turbostratic morphology. X-ray photoelectron spectra (XPS) of the catalyst precursors give binding energies for Ni $2p_{3/2}$ and $2p_{1/2}$ of 855.6 and 873.7 eV for BTP and 855.5 and 873.5 eV for PSP. These values contrast with those for catalysts prepared by impregnation using $Ni(NO_3)_3$ where the respective binding energies were, 856.0 and 874.3 eV in bentonite and 856.3 and 874.3 eV in palygorskite. The lower values obtained for the precipitated catalysts used here would suggest that nickel is bonded with a higher degree of covalent character, consistent with the presence of a nickel hydrosilicate, than in the case of impregnated catalysts where nickel will be present as the nitrate. The binding energy of 855.6 eV is

(17) Caillere, S.; Henin, S. *The X-Ray identification and crystal structures of clays minerals*; Brown, G., Ed.; Mineral Society: London, 1961; p 343.
(18) Gregg, S. J.; Sing, K. S. *Adsorption Surface Area and Porosity*; Academic Press: London, 1982.
(19) Richardson, J. A.; Dubus, R. J. *J. Catal.* 1978, *54*, 207.
(20) Montes, M.; Soupart, J.-B.; Saedeleer, M.; Hodnett, B. K.; Delmon, B. *J. Chem. Soc., Faraday Trans. 1* 1984, *80*, 3209.
(21) Martin, G. A.; Imelik, B.; Prettre, M. *C. R. Acad. Sci., Ser. C* 1967, *264*, 1536.

in exact agreement with the value reported by Vedrinne et al.[22] for nickel antigorite. From TPR studies conducted here and elsewhere[20,23] using the catalysts precursors, temperatures of at least 773 K are required for reduction of nickel contained in such phases. The process probably involves decomposition of the nickel silicate to the oxide followed by reduction to the metal.[19] Derivatives of temperature-programmed thermogravimetric experiments conducted in a flow of hydrogen show a maximum in weight loss for both samples at 623 K. However, for PSP, this maximum is followed by a tail terminating at 723 K, whereas for BTP a slight but definite continual weight loss was observed upto 973 K. The latter may in part be attributed to structural losses, but would also indicate the presence of a difficult to reduce phase present for BTP. Additionally, the calculated degree of reduction of the active phase (α) for catalysts reduced at 773 K, according to the procedure used prior to catalytic reaction, was less for catalyst BTP, indicating the presence of nickel in an additional phase to the antigorite, which is strongly interacting with the support. This would suggest that during preparation, a degree of substitution of Ni for Mg occurs in the montmorillonite. Nickel was essentially completely reduced in the palygorskite sample. This was confirmed in the IR spectrum of adsorbed CO for both samples. The spectrum of PSP (Figure 2B(a)) shows no bands in the region 2200–2100 cm^{-1} which would be indicative of incompletely reduced nickel species.[24] In contrast, a band appearing at 2193 cm^{-1} for BTP (Figure 2A(a)) may be assigned to CO adsorbed at isolated Ni^{2+} sites or at exposed Ni ions in oxidic type particles,[24–26] the former assignment being the more likely here. A further maximum in this region, at 2132 cm^{-1}, would also indicate CO adsorption at Ni sites in an oxidation state higher than zero, possibly Ni^{+}.[24] In this respect, spectra in this region are consistent with those obtained for Ni exchanged in, for example, mordenites, where the exchanged nickel may coexist in both Ni^{2+} and Ni^{+} states after mild reduction, giving bands at ca. 2200 and 2130 cm^{-1} due to adsorbed CO.[27] The detection of unreduced nickel centers by adsorption of CO is in disagreement with the model proposed by Coenen[6] who suggests that the unreduced nickel is present as a single antigorite layer which exists at the interface between nickel crystallites and the silica support. Such a model would not expose nickel ions to CO in the gas phase and hence not give rise to the infrared bands at 2132 and 2193 cm^{-1} as detected here (Figure 2A(a)).

Analysis of the spectra in the region 2100–2000 cm^{-1}, where CO adsorbed in the linear mode on reduced Ni atoms is detected, was hampered by the presence of a band at 2057 cm^{-1} due to $Ni(CO)_4$.[28] Although spectra shown were obtained by subtraction of the gas phase (which clearly shows a band at 2057 cm^{-1} in addition to the P and R branches of CO gas), the presence of $Ni(CO)_4$ interacting with the surface of the catalyst wafer prevents complete substraction of this maximum. The fact that this species is more frequently observed for low dispersed Ni samples[28] and low index crystal planes than for low concentrated

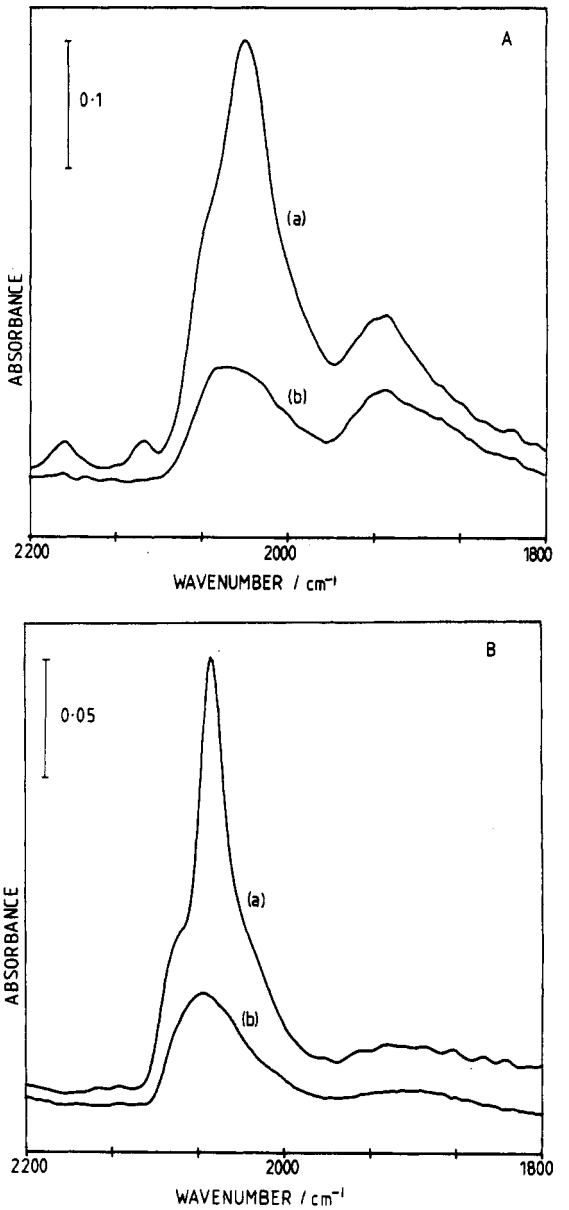

Figure 2. Infrared spectra of reduced catalysts (A) BTP and (B) PSP after (a) exposure to CO (2.0 kN m^2) at 300 K and (b) following evacuation at 300 K for 1 min.

supported Ni[24] would be consistent with the detection of the species here for a particle of ca. 10 nm diameter (Table III) which would display essentially bulk metal character and expose metal atoms in C_9 coordination, with low index planes such as Ni(111) being predominant.[28] However, in addition to the maximum attributed to nickel tetracarbonyl, spectra clearly show distinct shoulders at ca. 2085 and 2020 cm^{-1} which may be assigned to linearly bound CO at Ni^0 sites. Evacuation to remove $Ni(CO)_4$, weakly bound CO, and CO(g), shows this feature more clearly, in both cases producing a maximum at ca. 2060 cm^{-1} (Figure 2.A,B(b)). The particle sizes as determined by TEM and XRD line broadening (Table III) show a good correlation between both techniques and indicate that the average particle size in both supports is approximately equal. Electron micrographs indicate a homogeneous distribution of particles over both supports and that the particle sizes range between 90 and 110 Å. The ratio of linear (2100–2000 cm^{-1}) to bridge (2000–1800 cm^{-1}) bound carbonyls is related to the metal crystallite size,[25,26] with the bands in the lower frequency region being more abundant for smaller particle sizes containing a higher proportion of Ni

(22) Vedrinne, J. C.; Hollinger, G.; Duc, T. M. *J. Phys. Chem.* **1978**, *82*, 1515.
(23) Martin, G. A.; Mirodatos, C.; Praliaud, H. *Appl. Catal.* **1981**, *1*, 367.
(24) Peri, J. B. *J. Catal.* **1984**, *86*, 84.
(25) Primet, M.; Dalmon, J. A.; Martin, G. A. *J. Catal.* **1977**, *46*, 25.
(26) Wielers, A. F. H.; Aaftink, G. J. M.; Geus, J. W. *Appl. Surf. Sci.* **1985**, *20*, 564.
(27) Garbowski, E. D.; Mirodatos, C.; Primet, M. In *Studies in Surface Science and Catalysis*; Jacobs, P. A., Jaeger, N. I., Jiru, P., Schultz-Ekloff, G., Eds.; Elsevier: Amsterdam, 1982; Vol. 12, p 235.
(28) van Hardeveld, R.; Hartog, F. *Appl. Catal.* **1972**, *22*, 75.

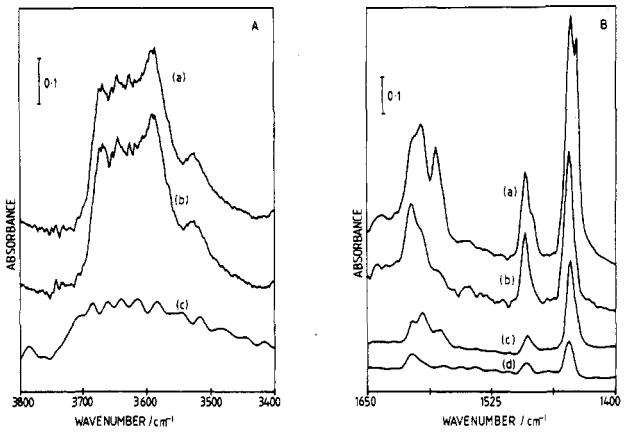

Figure 3. Infrared spectra of pyridine adsorption on catalyst samples: (A) OH region for PSP (a) before and (b) after exposure to C_6H_5N (2.0 kN m^2), and (c) for BTP prior to C_6H_5N adsorption; (B) (a) BTP following exposure to C_6H_5N (2.0 kN m^2) and (b) after evacuation at 300 K for 10 min. (c) PSP following exposure to C_6H_5N (2.0 kN m^2) and (b) after evacuation at 300 K for 10 min.

atoms with coordination less than 9.[28] As shown in parts A and B of Figure 2, catalyst BTP clearly contains the greater proportion of bridging carbonyls, with the maximum at 1945 cm^{-1}. As sample BTP contains the larger average particle size (Table III), this may be interpreted as an indication that BTP also contains a proportion of small particles which are not detected by these techniques. This would be consistent with the difficulty in completely reducing nickel in the BTP sample indicating a strong interaction with the support and preventing sintering during heat treatment in hydrogen at elevated temperatures. The presence of these small crystallites is consistent with the expectation of reduction of nickel exchanged into the montmorillonite matrix. From the average particle sizes measured by TEM, and taking into acocunt the proportion of unreduced nickel, the approximate metallic surface areas were calculated and are shown in Table III. Due to the presence of small particles in the BTP catalyst, the error involved in calculating the metal area will be greater for this sample.

The total acidity in the form of micromoles of pyridine adsorbed per gram of support was found to be greater in the case of BTP. This was consistent with the infrared data which shows that bands due to adsorbed pyridine were of greater intensity for BTP than for PSP (Figure 3B), taking into account the relative weight of the samples used. In both samples, bands were observed at 1447, 1490, and 1606 cm^{-1} following evacuation of physically adsorbed pyridine, and indicative of pyridine chemisorbed at exposed Lewis acid sites in the support surface.[29] The absence of maxima at ca. 1540 and 1640 cm^{-1} would indicate that Brønsted acid sites are not present for either material although Brønsted acidity has been detected for palygorskite samples after outgassing at 423 K.[30] Sample BTP shows only a weak broad maximum in the OH stretching region of the spectrum (Figure 3A) whereas hydroxyl species are readily observed in the case of PSP with maxima at 3668, 3645, 3592, and 3528 cm^{-1} (Figure 3A(a)). These are in agreement with bands at 3660, 3640, 3585, and 3525 cm^{-1} reported for the unloaded palygorskite.[30] However for the nickel-containing support here, and in contrast to behavior for the support alone,[30] these maxima were not perturbed by the presence of pyridine (Figure 3A(b)) indicating that these hydroxyls are incorporated into the bulk of the support or that they are located in pores which are inaccessible to the pyridine molecule. Perturbation of the former band pair, attributed to hydroxyls in the folded material, was attributed to the unfolding of palygorskite as a result of pyridine entering its channels.[30] The absence of interaction between these hydroxyls and pyridine here, as also observed for Al-exchanged sepiolite degassed at 623 K[31] may be the result of the structural modifications resulting from incorporation of nickel (Table II) or to the irreversible folding resulting from the pretreatment at 673 K. The pair of bands at 3592 and 3528 cm^{-1} may be attributed to coordinated water on octahedral Mg or at an exchanged cation in this position.[30,31] Previously reported bands due to hydroxyl species at *ca.* 3430 and 3225 cm^{-1} for palygorskite[30] were not observed here, although an additional pair at 3378 and 3300 cm^{-1}, not shown in Figure 3A, was detected. These were also unperturbed in the presence of pyridine. The inaccessibility of all of these forms of hydroxyl species to pyridine, whether Brønsted acidic or otherwise, indicates that they may be neglected as having any role in the hydrogenation reaction of the triglycerides.

Catalytic Activity and Selectivity. For the hydrogenation of polyunsaturated fatty acids, two types of centers may be involved: (1) Lewis acidic centers where the triglyceride molecule is adsorbed via the double bond and (2) reduced metal sites for the dissociation of molecular hydrogen.[32,33] In such a case, the degree of reduction of the metal (α), the metal surface area (S_{Ni}), and the number of Lewis acidic centers on the catalyst surface are factors which may influence catalytic activity. The activity in mol/(L min) per gram of Ni was 30.5×10^{-2} for the catalyst BTP and 38.2×10^{-2} in the case of catalyst PSP. As the acidity of the catalyst BTP was greater than in the palygorskite sample, the role of the acid centers in determining the differences in activity[32,33] between the two catalysts may be neglected. When catalyst activity is calculated by taking into account the degree of reduction for each catalyst, the values are 35×10^{-2} and 39×10^{-2} mol/(L min g) for BTP and PSP, respectively. As fatty acid hydrogenation is a structure-insensitive reaction, the catalytic activity should be proportional to nickel surface area. Coenen[6] attributed the absence of correlation between crystallite size and activity to the presence of part of the nickel surface area being insufficiently accessible to the triglyceride molecule, with nickel in pores of 20 Å or less playing no part in the reaction. Although the detection here of particles not detected by TEM using infrared spectroscopy of adsorbed CO would indicate a higher metal surface area for BTP than that calculated from the mean particle size, these particles will make no contribution to catalytic activity if located in pores which are inaccessible to the reactant molecule. The insignificant differences between catalytic activity here indicates that these small Ni particles in the BTP catalyst may be located in sites where the contribution of nickel to the overall hydrogenation of linoleic acid is negligible.

In defining the selectivity here, the formation of oleic acid as the desired product of the hydrogenation of sunflower oil is considered. Figure 4 shows the selectivity to oleic acid and indicates that there are significant differences between the two catalyst. For palygorskite (PSP catalyst) the selectivity is 95% at a conversion level

(29) Parry, E. P. *J. Catal.* **1963**, *2*, 371.
(30) Blanco, C.; Herrero, J.; Mendioroz, S.; Pajares, J. A. *Clays Clay Miner.* **1986**, *36*, 364.
(31) d'Espinose de la Caillerie, J.-B.; Fripiat, J. J. *Catal. Today* **1992**, *14*, 125.
(32) Sarier, S.; Gùller, C. *J. Am. Oil Chem. Soc.* **1989**, *66*, 917.
(33) Pavlenco, N. V.; Tripol'skii, A. I.; Popovich, O. T.; Golodets, G. I. *Kinet. Catal.* **1989**, *30*, 744.

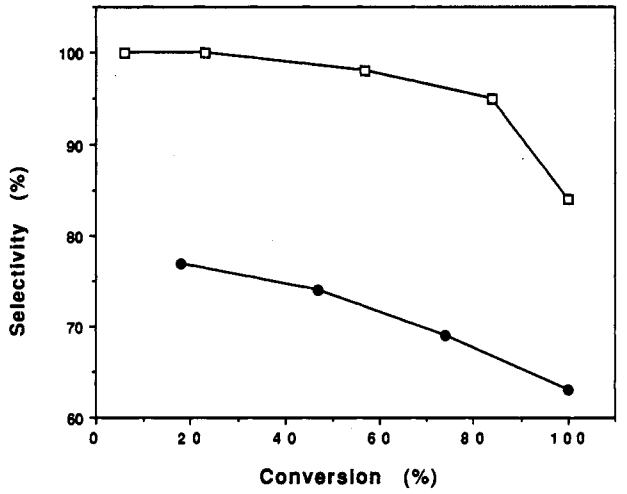

Figure 4. Selectivity to oleic acid as a function of percentage conversion of linoleic acid over catalysts BTP (●) and PSP (□).

of 85%, whereas on bentonite (BTP catalyst) the selectivity is less than 75% even at the very low conversion of about 30%, and 66% for a conversion level of 85%. The initial 100% selectivity to oleic acid over PSP is in agreement with previous reports[6,34] which state that linoleic acid is hydrogenated preferentially and faster than oleic acid. The pore size has been shown to be of crucial importance in determining the selectivity[6,7,35] with active surface in pores between 20 and 35 Å giving poor triglyceride selectivity as a result of mass transport problems.[6] This leads to an accumulation of the partially hydrogenated product in such pores and consequently to a depression of selectivity. The selectivity of nickel on the different supports here may be explained, not as a function of relative pore sizes but as a function of their different morphologies. In the case of bentonite, linoleic acid may enter the enlarged slit-shaped pores between lamellae, resulting from a combination of swelling and delamination of the original clay. The active phase held within such areas will therefore be exposed to triglyceride molecules in a confined environment, hindering the transport of the partially hydrogenated molecule and leading to an accumulation of oleic acid between lamellae. Consequently the reaction will proceed through to stearic acid. For the palygorskite support, bonding between fibers will be much weaker in nature and may be broken by agitation during reaction. This will leave Ni exposed in less confined environments (i.e. a higher proportion of active Ni surface is external) allowing transport of the partially hydrogenated product away from the active centers.

(34) Grau, J. G.; Cassano, A. E.; Baltanas, M. A. *Catal. Rev.-Sci. Eng.* **1988**, *30*, 1.
(35) Kõseoglu, S. S.; Lusas, E. W. *J. Am. Oil Chem. Soc.* **1990**, *67*, 39.